Numerical Methods in Civil Engineering, 6-2 (2021) 77-92

**Numerical Methods in Civil Engineering**

Journal Homepage: https://nmce.kntu.ac.ir/

# Fragility analysis of nonlinear soil-structure systems including foundation uplifting and soil yielding

**Hamid Masaeli*, Masoud Ahmadi****

*ARTICLE INFO*

RESEARCH PAPER

*Article history:*
*Received:*
*May 2021.*
*Revised:*
*July 2021.*
*Accepted:*
*August 2021.*

*Keywords:*
*Soil-structure interaction;*
*Seismic fragility curve;*
*Earthquake loss estimation;*
*Steel MRF;*
*Nonlinear dynamic analysis.*

***Abstract:***

*The present study is focused on fragility analysis of steel moment resisting frames (MRFs) incorporating nonlinear soil-structure interaction (SSI) effects. To this end, incremental dynamic analyses are performed using a suit of real ground motion records. A MRF structure is considered which is supported by single footings. To evaluate the SSI effects, four cases are compared including (i) fixed base, (ii) linear SSI and uncoupled footings (i.e. without tie beams), (iii) nonlinear SSI and uncoupled footings and (iv) nonlinear SSI and coupled footings (i.e. with tie beams). The SSI effect is represented by modified Beam-on-nonlinear Winkler foundation (BNWF) model. An appropriate structural damage index based on summation of cumulative plastic hinges' rotations is employed. The seismic fragility curves of the structures are derived and compared for the above-mentioned cases. The results show that nonlinear SSI has significant effects on seismic fragility curves. Evidently, these effects are mitigating especially in case of footings with tie beams. To assess the effect of ground motion type, fragility curves are also derived for each type of ground motion comparatively. It is observed that near field pulselike records are more destructive than far field or near field no-pulse records in terms of fragility curves. Overall, based on findings of this study, the obtained modified fragility curves are supposed to be helpful for the earthquake engineers to conduct more realistic loss estimations considering SSI effects. These modification factors need to be generalized with respect to a variety of structural systems, site types and foundation configuration.*

## 1. Introduction

One of the pillars of earthquake preparedness is to provide a seismic loss estimation platform in order to predict the consequences of an uncertain earthquake to civil infrastructure. Application of fragility curves is known as a solution to overcome the highly unpredictable nature of the problem in seismic hazard programs. Fragility is a term that describes the probability of failure to meet a performance objective as a function of demand on the system. The earliest widespread application of fragility analysis against earthquake demands was provided in ATC-13 [1]. The well-known program for loss estimation, HAZUS [2], developed under Federal Emergency Management Agency (FEMA) sponsorship, incorporates fragilities for 36 categories of building and four damage states.

* *Assistant Professor, Department of Civil Engineering, Ayatollah Boroujerdi University, Boroujerd, Iran.*
** *Corresponding author: Assistant Professor, Department of Civil Engineering, Ayatollah Boroujerdi University, Boroujerd, Iran, Email: masoud.ahmadi@abru.ac.ir.*

Both ATC-13 and HAZUS are based to a great extent on engineering judgements.

More recent approaches have relied more on computational bases. In the new paradigm of consequence-based risk management (CBRM) performance assessment tools are being developed for use in seismic risk reduction. The fragility of components or systems is a key element of this process, as it not only defines the probability of reaching target damage states as a function of a specified measure of earthquake ground motion intensity but is also required for estimating expected or maximum probable losses. Several studies [3-5] in the literature are devoted to seismic fragilities of several typical low-to-mid-rise steel and reinforced concrete buildings representative of design and construction practices. A comparison of these fragilities, based on nonlinear time history analyses (NTHAs), with those incorporated in HAZUS indicates that the fragilities from HAZUS tend to be quite conservative in predicting collapse in comparison with those computed through a more sophisticated NTHA-based assessment, particularly for the steel frames. Accordingly, the drift limits implied in the

HAZUS fragilities are conservative (4-5% in HAZUS vs 9-10% from NTHAs [6]), and the logarithmic standard deviations are substantially higher, often exceeding 90%, while those from NTHAs are on the order of 50% or less [6]. However, it should be noted that HAZUS is aimed at regional loss estimation rather than building-specific vulnerability assessment, and the large logarithmic standard deviations are due to considerable variation on construction details within each building category.

In general, fragility curves can include several sources of uncertainties: in the seismic loading, the soil site and the structural parameters defining the system. From a modern fragility modeling perspective, there is increasing demands for the analysis of epistemic uncertainties. In contrast, the notions of building fragility and vulnerability assessment, in current form, are not well established in dealing with dynamic soil-structure interaction (SSI) effects, as one of the sources of uncertainties. To fill this gap and achieve more reliable loss estimation, there have been some attempts recently to develop the fragility modeling of the buildings incorporating SSI effects (e.g. [7]). As a step toward considering SSI effect, Saez et al. [8] have studied the influence of nonlinear SSI on the seismic vulnerability assessment of a typical building with surface raft foundation. The seismic vulnerability was evaluated in terms of analytical fragility curves constructed on the basis of NTHAs. The developed fragility curves were compared with reference curves in HAZUS. Concerning the effect of the nonlinear SSI, a general reduction of seismic demand was found in the derived fragility curve. Saez et al. have postulated that the observed reduction in seismic demands can be associated fundamentally to two phenomena: radiation damping and hysteretic damping due to nonlinear soil behavior. However, they also explained that, inelastic SSI could increase or decrease the seismic demand depending on the type of structure, the input motion characteristics and the dynamic soil characteristics. Overall, the main drawback of their study is neglecting the inelastic behavior within superstructure domain. In consequence, they had no choice but to limit their investigations to slight-to-moderate damage states. Consequently, observations of structural fragilities prior to collapse could not be accomplished.

To simulate nonlinear SSI including foundation uplifting and soil yielding, three different approaches exist in the literature. Firstly, direct method is a well-known approach within which the underlying soil elements are directly constructed using the continuum solid elements, and the consistent soil behavioral model is attributed to the soil elements. Secondly, macroelement approach is another method through which the nonlinear inelastic behavior of foundation-soil is analytically encoded within a composite element namely “macroelement” which is assigned to the base node of first-story columns of structure. Thirdly, Beam-on-Nonlinear Winkler Foundation (BNWF) model is a well-known and suitable method which provides reasonable accuracy in terms of moment-rotation behavior of shallow foundations. This model, which is employed in the present study, is verified and calibrated on the basis of an extensive experimental data. In the meantime, the BNWF model is advantageous in terms of computational efforts in comparison with direct method.

This study is mainly focused on seismic damage assessment of low-rise steel moment resisting frames (MRFs) while SSI effects are included. The inelastic behavior of superstructure is considered and consequently higher damage states can be evaluated. A five-story MRF structure is selected as representative of building inventory in Iran, where the structure is supported by single footings. The SSI effect is represented by modified Beam-on-nonlinear Winkler foundation (BNWF) model. Incremental dynamic analyses (IDAs) are performed using a suit of real ground motion records. An appropriate structural damage index based on summation of cumulative plastic hinges’ rotations is employed. The seismic fragility curves of the structures are derived and compared for different SSI conditions. The four comparative SSI conditions include fixed base, linear SSI, and nonlinear SSI (i.e. foundation uplifting and soil yielding are considered). The foundation system in nonlinear SSI condition is supposed to be with or without tie beams.

## 2. Building Inventory

The basic elements for conventional pre-event seismic loss estimation can be stated as the estimation of the surface ground motion, the compilation of the city inventory, the development of the vulnerability functions or structural fragility curves, and the implementation of a method in calculating and then evaluating the losses. Metropolitan area of greater Tehran is chosen as the area of interest, keeping in mind that the process is applicable for the entire region. The vulnerability of this area was studied first by the Centre for Earthquake and Environmental Studies of Tehran and the Japan International Cooperation Agency (JICA) in 2000 [9], based on the data collected before the year 2000 in the form of city blocks.

JICA used the building data from 34,805 census blocks as provided by the Iranian Census Center. The survey of the building infrastructure in Tehran, Iran [10] revealed that buildings with steel and RC structural systems comprise approximately 1% of the total building inventory, and that the steel frames comprise 72% out of the total 1%. The vast majority of these buildings (over 85%) is five stories in height or less and was constructed prior to 1990. Since steel and concrete frames are significant for commercial and industrial occupancies, the focus of the current study is on

such frames. Regarding to the fact that steel frames are more widespread compared to RC frames, a typical 5-story frame is selected to be representative of construction in Tehran.

## 3. Superstructure Description

A 5-story steel frame is selected from three-dimensional structural modeling in which, plans are considered symmetric and similar, to avoid the effects of geometrical asymmetry. As depicted in Fig. 1a, each frame constitutes of three identical spans, and story height in all of them is 3.2 m. The width of spans is 6.0 m and the aspect ratio of the frame is 0.89. Lateral seismic resisting system is a special steel moment-resisting frame. For loading of structures, ASCE7-10 [11] is considered, and the design dead and live loads are 550 and 200 kg/m$^2$, respectively. These gravity loads are distributed over the floor using a chessboard loading pattern. Structures are designed in fixed-base condition in accordance with the American Institute of Steel

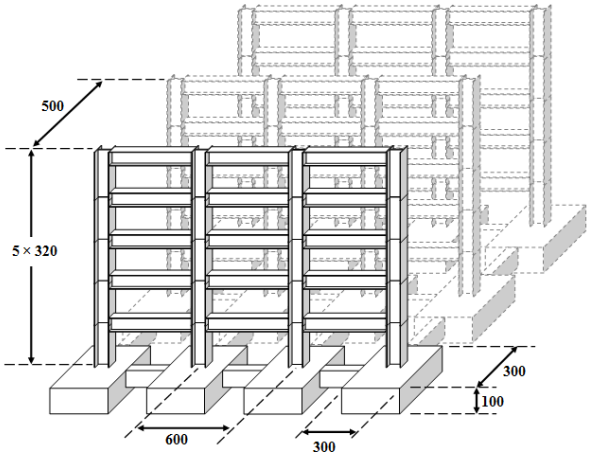


(a)

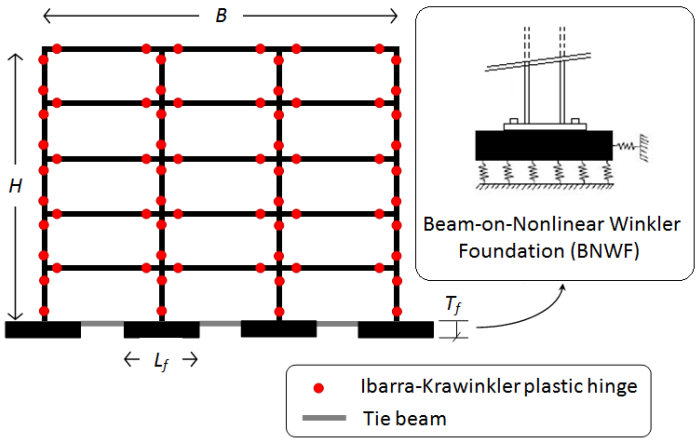


(b)

**Fig. 1:** a) 3D view of the primary building-foundation system; b) Soil-foundation-structure model

**Table. 1:** Section properties of the designed MRF structure and modal periods

| Story | Sections | | Modal periods | |
|---|---|---|---|---|
| | Column | Beam | $T_1$ (s) | $T_2$ (s) |
| 1-5 | HEB 320 | IPE 360 | 1.35 | 0.41 |

Construction AISC-10 [12]. Linear static and linear spectrum methods are employed for designing the frames using commercial software.

Steel profiles are all A36 with yielding strength of 2500 kg/cm$^2$, ultimate strength of 4070 kg/cm$^2$ and elasticity modulus of 2,100,000 kg/cm$^2$. Its Poisson's ratio is 0.3 and its density is equal to 7833 kg/cm$^3$. Loading assumptions required in the ASCE7-10 are as follows. Seismic zone is assumed to be zone 4, which includes the near-fault effects. Soil type is considered stiff soil (SD) (as per the code's instructions, we can assume the soil type to be SD when no information is available). Occupancy factor (I = IP) is considered 1. Moreover, 0.2 and 1 s spectral response accelerations ($S_s$ and $S_1$) are considered 1.5 and 0.6,

respectively. Thus, values of site coefficients ($F_a$ and $F_v$) will be 1 and 1.5. Table 1 shows the section properties of the designed members as well as first- and second-mode periods of the constructed fixed-base model. Once the frame sections are designed assuming fixed-base superstructure, this study aims to assess seismic performance of the soil-foundation-structure system. The open-source program OpenSees [13] developed in the Pacific Earthquake Engineering Research (PEER) Center, is used to model the frame for NTHAs. The nonlinear behavior is represented using the concentrated plasticity concept with rotational springs. The rotational behavior of the plastic regions follows a bilinear hysteretic response based on the Modified Ibarra-Krawinkler Deterioration Model [14,15]. The bilinear steel behavior is assumed with secondary stiffness equal to 3%. A leaning column carrying gravity loads is linked to the frame to simulate P-Delta effects. Also, Rayleigh damping model was used, in which the damping ratio was assumed to be 2% of the critical damping for the first and fourth modes.

## 4. Soil-Foundation Modeling

The beam-on-nonlinear-Winkler foundation (BNWF) model is used in this study to simulate nonlinear soil-foundation interaction. This model was proposed by Gajan et al. [16] and earlier by Harden and Hutchinson [17] and Harden et al. [18]. The BNWF model is also integrated with the openly available software platform OpenSees [13] by Raychowdhury and Hutchinson [19]. BNWF model with nonlinear springs of variable stiffness intensity can characterize the nonlinear time dependent behavior of the foundation-soil interface, for shallow foundations (footings, mats). These composite nonlinear springs, representing the underlying soil, are schematically displayed in Fig. 1b.

The BNWF model integrated with OpenSees, namely "ShallowFoundationGen" module, consists of elastic beam-column elements that capture the structural behavior of foundation as well as independent zero-length soil elements to model the soil-foundation interaction. The modified BNWF model is verified and calibrated using an extensive experimental data. Further details on BNWF model are available in PEER Report 2007/04 [18]. The parameters required for the BNWF model are related to soil and footing properties in addition to finite element mesh properties. The finite element mesh properties include stiffness intensity ratio of vertical springs (Rk), end length ratio (Re), which is defined as width of end length high-stiffness region divided by total footing length, and lastly, vertical spring spacing (Se) as a fraction of total footing length. Parameters of particular interest describing geotechnical properties of the subsoil are set corresponding to soil type III in accordance with Iranian seismic code, Standard 2800 (corresponding to soil type D based on site classification introduced in ASCE7-10). The foundation system is assumed to be single footing with and without tie beams comparatively. The input parameters of the BNWF model are presented in Table 2.

Three comparative SSI conditions are considered in this study: first, "fixed-base" condition, that means the foundation system and supporting soil are rigid; second, "linear SSI" condition, that means flexible foundation and soil but not allowed to uplift and no soil yielding; third, "nonlinear SSI" condition in which foundation uplifting and soil plasticity are included.

## 5. Input Ground Motion

The seismic performance of the soil-foundation-structure system is investigated through nonlinear dynamic time history analyses. An ensemble of 27 real accelerograms is used as a subset of near-field as well as far-field records recommended by FEMA-P695 [21]. Fig. 2 illustrates the ground acceleration histories of the selected ensemble. Of the entire 27 accelerograms, twelve records are classified as near-field pulse-like, as judged by wavelet analysis classification [22], eight are classified as near-field no-pulse records, and the remaining seven are classified as far-field records.

To assess the effects of ground motion intensity, the suite of near-field records used in this study is scaled with respect to design spectrum introduced in Iranian seismic code, Standard 2800 [23]. The Standard 2800 guidelines define two levels of earthquake shaking hazard, termed Design Basis Earthquake (DBE) and Maximum Credible Earthquake (MCE). DBE is defined as a ground shaking with 10% probability of surpassing in 50 years. MCE ground shaking has 2% probability of surpassing in 50 years. Earthquake shaking demand on buildings is characterized by acceleration response spectra for these two hazard levels.

Ground motion record scaling is performed as recommended in FEMA-p695 [21]. Accordingly, record scaling involves two steps. First, individual records in each set are normalized by their respective peak ground velocities (PGVs). This step is intended to remove unwarranted variability between records due to inherent differences in event magnitude, distance to source, source type and site conditions, without eliminating overall record-to-record variability. In this study, the selected record set is normalized so that PGV is set equal to 50 cm/s. The ground acceleration histories of the normalized records are depicted in Fig. 2. Second, the normalized ground motions are collectively scaled to a specific ground motion intensity such that the median spectral acceleration of the record set matches the spectral acceleration at the fundamental period, *T*, of the index archetype that is being analyzed.

Fig. 3 displays 5% damped elastic pseudo-acceleration response spectra (PSa). Computed PSa envelope, mean PSa,

standard deviation ( $\sigma$ ) and reference spectrum for soil class III in seismic zone of very high seismic hazard according to categorization of Iranian seismic design guidelines Standard 2800 [23], presented in this figure. Generated ground motions spectra displayed in Fig. 3 are compared to the Iranian seismic design spectrum (Standard 2800). Spectral ordinates of mean spectrum for periods around $T_1$=1.35 s approximately coincide with those of the design spectrum. For periods other than 1.35 s, spectral ordinates are in general slightly less than those of the design spectrum.

## 6. Dynamic Time-History Analyses

Consider the 5-story steel MRF structure as described in section 3. The boundary condition of the structure is assumed to be (i) fixed base, (ii) linear SSI and uncoupled foundation (i.e. without tie beams), (iii) nonlinear SSI and uncoupled foundation, and (iv) nonlinear SSI and coupled foundation (i.e. with tie beams). These boundary conditions are denoted by Case 1 through 4, in the same order. The seismic performance of the four alternatives is investigated through NTHAs. An ensemble of 27 real accelerograms is used as seismic excitation of the soil-foundation-structure system, as described in previous section. In all cases, the seismic excitation is applied at the far ends of the zero-length elements at the boundaries, as displayed schematically in Fig. 1b. In the following sections, the SSI effects on displacement as well as force demands of the superstructure are typically investigated, when the soil-foundation-structure system is subjected to an individual ground motion.

**Table. 2:** Input parameters of the BNWF model

| | |
|---|---|
| **Geotechnical properties of the subsoil** | |
| Cohesion, $C$ (KN/m$^2$) | 14.7 |
| Friction Angle, $\phi$ (deg) | 30 |
| Shear Modulus, $G$ (MPa) | 657.7 |
| Poisson's Ratio, $\nu$ | 0.35 |
| **Geometrical and structural properties of the footings** | |
| Footing Length, $L$ (m) | 3.0 |
| Footing Width, $B$ (m) | 3.0 |
| Footing Thickness, $t$ (m) | 1.0 |
| Elastic Modulus of Concrete, $E$ (GPa) | 23.4 |
| Tie Beam Width, $b$ (m) | 0.3 |
| Tie Beam Height, $h$ (m) | 0.5 |
| **Mesh parameters of the BNWF model** | |
| Stiffness Intensity Ratio of Vertical Springs, $R_k$ | 1.95 |
| End Length Ratio, $R_e$ | 0.08 |
| Vertical Spring Spacing Ratio, $S_e$ | 0.04 |

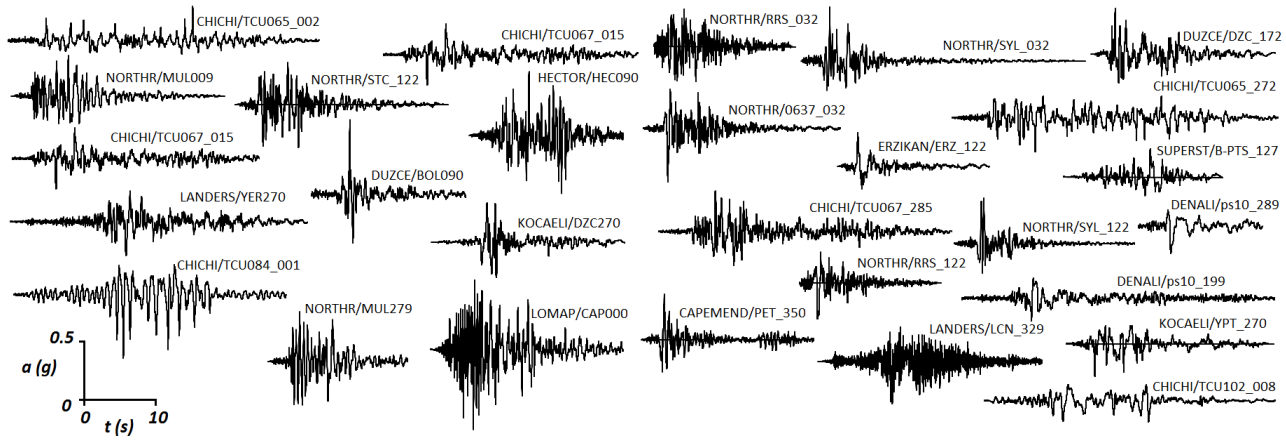


**Fig. 2:** Ground acceleration histories of the normalized records

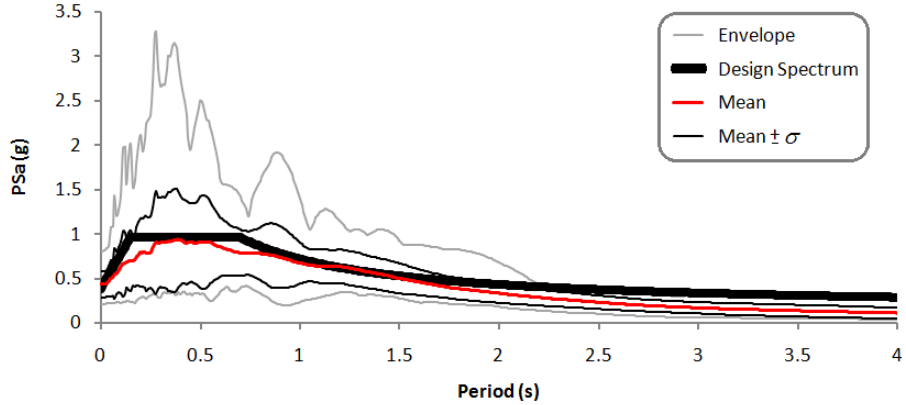


**Fig. 3:** Scaling of the normalized records based on the Iranian seismic design spectrum (Standard 2800).

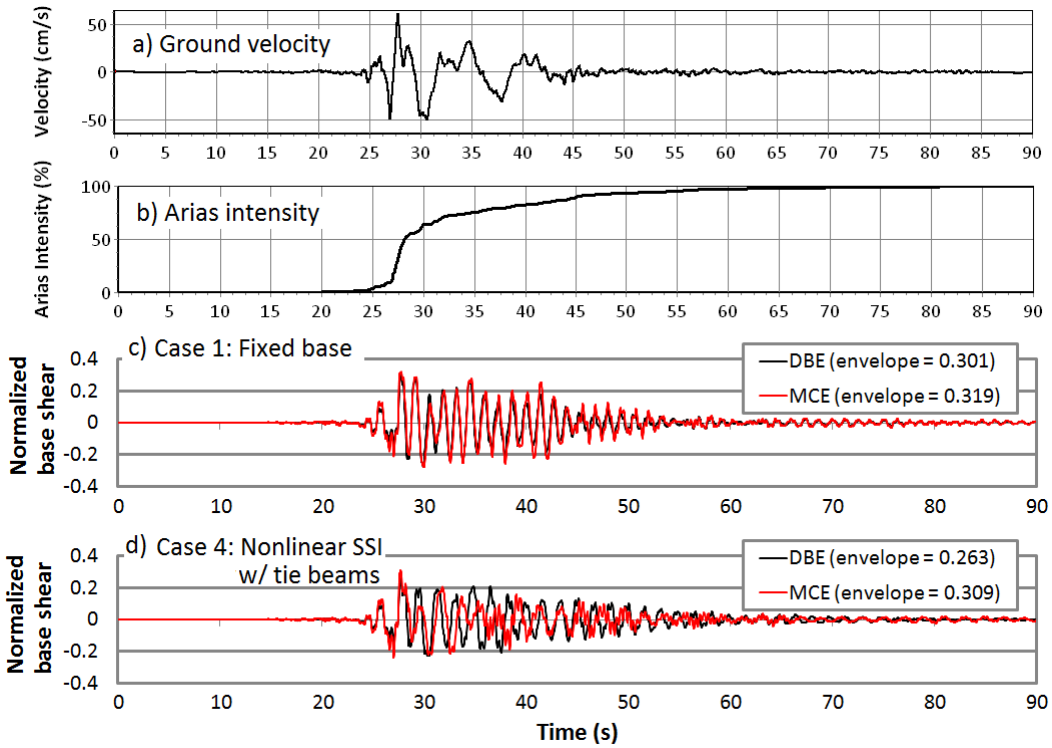


**Fig. 4:** Time-history of normalized base shear in two different SSI conditions

### *6.1. SSI effects on force demands*

The SSI effect on force demands of the building is investigated at two different excitation levels. Normalized base shear, defined as base shear divided by total weight of the superstructure, is selected as quantitative index of the structural force demands. The two excitation levels are selected as design basis earthquake (DBE) and maximum credible earthquake (MCE). The latter is defined as 1.5 times the DBE excitation level.

As an example, the normalized base shear histories are plotted in Fig. 4 when the frame is typically subjected to fault-normal component (ps10_199) of 2002 Denali, Alaska, TAPS Pump Sta. #10 ground motion. The time history of ground velocity is shown in Fig. 4a. The Arias intensity of the record is displayed in Fig. 4b to represent the rate of seismic input energy to the soil-foundation-structure system. The normalized base shear histories in cases 1 and 4 are given in Figs. 4c and 4d, respectively. The normalized base shear histories are plotted in pair corresponding to DBE (in black) as well as MCE (in red) excitation levels. The results show that the force demands are reduced in nonlinear SSI condition (case 4) especially at DBE level. So, the maximum absolute value of normalized base shear at DBE level is 0.301 in case 1 which is reduced to 0.263 in case 4. But the base shear is slightly reduced at MCE level. Overall, the results show that the SSI effects on force demands are not of great importance according to this individual NTHA. Bearing in mind that the spectral acceleration SA of a motion is not always the most crucial parameter of nonlinear response, the characterization of the seismic motions with respect to the surpassing design limits is conducted on the

basis of spectral displacements SD, following the logic of displacement-based design [24,25]. Accordingly, the SSI effects on displacement demands of the superstructure are discussed in the following section.

### *6.2. SSI effects on displacement demands*

The SSI effect on displacement demands of the building is investigated at DBE and MCE excitation levels. Interstory drift ratio (IDR), defined as the envelope of relative displacement between two consecutive story levels normalized by the story height, is used as the primary engineering demand parameter. In order to estimate the relative IDRs, the rigid-body interstory displacements caused by rocking behavior of the frame are extracted in cases 2 through 4. For this purpose, the average foundation tilting angles are computed among the four footings. Fig. 5 illustrates the distribution of IDRs over the height for the four SSI cases comparatively. The soil-structure system is subjected to fault-normal component (ps10_199) of 2002 Denali, Alaska, TAPS Pump Sta. #10 ground motion. The incident record is scaled to DBE (not exceeding design limits) as well as MCE (exceeding design limits) as given in Figs. 5a and 5b, respectively.

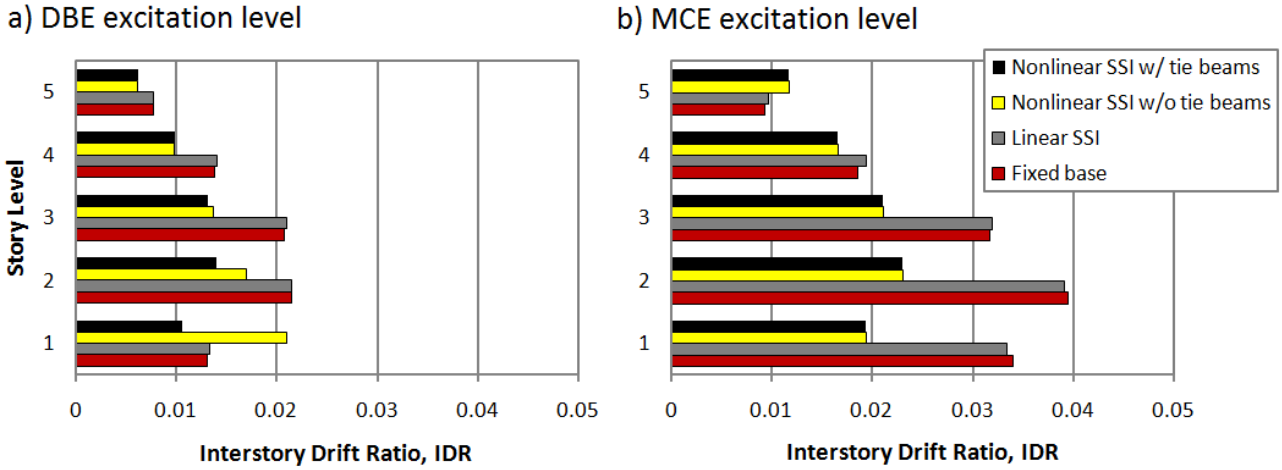


**Fig. 5:** SSI effects on drift demands at two different excitation levels

The results of Fig. 5a show that nonlinear SSI during the selected earthquake not exceeding design limits leads to significant reduction in drift demands, especially in middle stories. In contrast, the IDRs in case 3 are increased in lower stories so that the IDR of the base is significantly greater than cases 1 and 2. Meanwhile, the coupled performance of foundation with tie beams in case 4 at DBE level has noticeably improved the drift demands at lower stories i.e. IDR equal to 0.022 in case 3 is reduced to 0.011 in case 4. Fig. 5b shows that the gap between IDRs in cases 3 and 4 compared to cases 1 and 2 is widened when the excitation is intensified up to MCE, especially in lower stories. Evidently, the IDR is more uniformly distributed along height, when nonlinear SSI is incorporated. Yet, infinitesimal difference is observed between case 4 compared to case 3, which indicates that the superstructure's displacement demands are almost independent of the tie beams.

According to the thresholds introduced in HAZUS [2] for moderate-code mid-rise steel moment frames (S1M), the IDR equal to 0.0157 and 0.04 corresponds to extensive as well as complete structural damage states, respectively. Then, with regard to the typical results of Fig. 5b, it is demonstrated that the damage state of the superstructure from complete structural damage state in cases 1 and 2 is lowered to extensive damage in cases 3 and 4. This fact reveals the significant role of nonlinear SSI incorporation on seismic damage of the superstructure during earthquakes exceeding design limits. In addition, based on the obtained typical results, application of tie beams is another key factor which can affect the damage state of the building during earthquakes not exceeding design limits. Based on the observations, the nonlinear SSI incorporation and coupled performance of the foundation system due to tie beams are the two key factors which can potentially influence the estimated seismic damage of a building subjected to a given ground motion. Hence, these two factors are investigated in the NTHA-based fragility analysis of the steel frame in this study.

## 7. Nonlinearities in Soil-Foundation Response

The authors now take a closer look at the nonlinear response of the soil-foundation system when the foundation uplifting and soil yielding are considered (i.e. cases 3 and 4). For this purpose, time histories of foundation uplifting as well as foundation tilting are typically presented in Figs. 6 and 7, respectively. The footings are numbered from left to right and the soil-foundation structure system is subjected to the

same record of Fig. 4. The excitation level is DBE in parts (a) and (b) of Figs. 6 and 7. We then extend the comparison for a large intensity motion, exceeding the design limits in parts (c) and (d) of Figs. 6 and 7.

The results of Fig. 6 show that coupled foundation (i.e. with tie beams) exhibits greater uplifting than foundation without tie beams at both excitation levels.

As displayed, the maximum foundation uplifting is 140 and 240 mm in case of uncoupled foundation, while the corresponding values are increased up to 190 and 295 mm. It can be observed that coupled foundation subjected to strong earthquake beyond design limits undergoes considerable uplift (almost a foot).

The rocking behavior of the foundation is evaluated in terms of foundation tilting in Fig. 7. The foundation tilting histories portray the formation of plastic hinges at substructure level. More precisely, the residual foundation tilting at the end of the time history represents the plastic hinge within the underlying soil. Accordingly, the results of Fig. 7 show that coupled foundation exhibits more integrated rocking behavior, and the residual foundation tilting is controlled within reasonable limits. On the contrary, the exterior footings without tie beams undergo excessive residual foundation tilting which has obtained almost equal to 0.025 rad in worst case. Such extensive plastic hinging within the underlying soil can lead to serious serviceability problems for the structure surviving a strong earthquake beyond the design limits. By application of the tie beams, the maximum residual foundation tilting has decreased to 0.01 rad in case of coupled foundation.

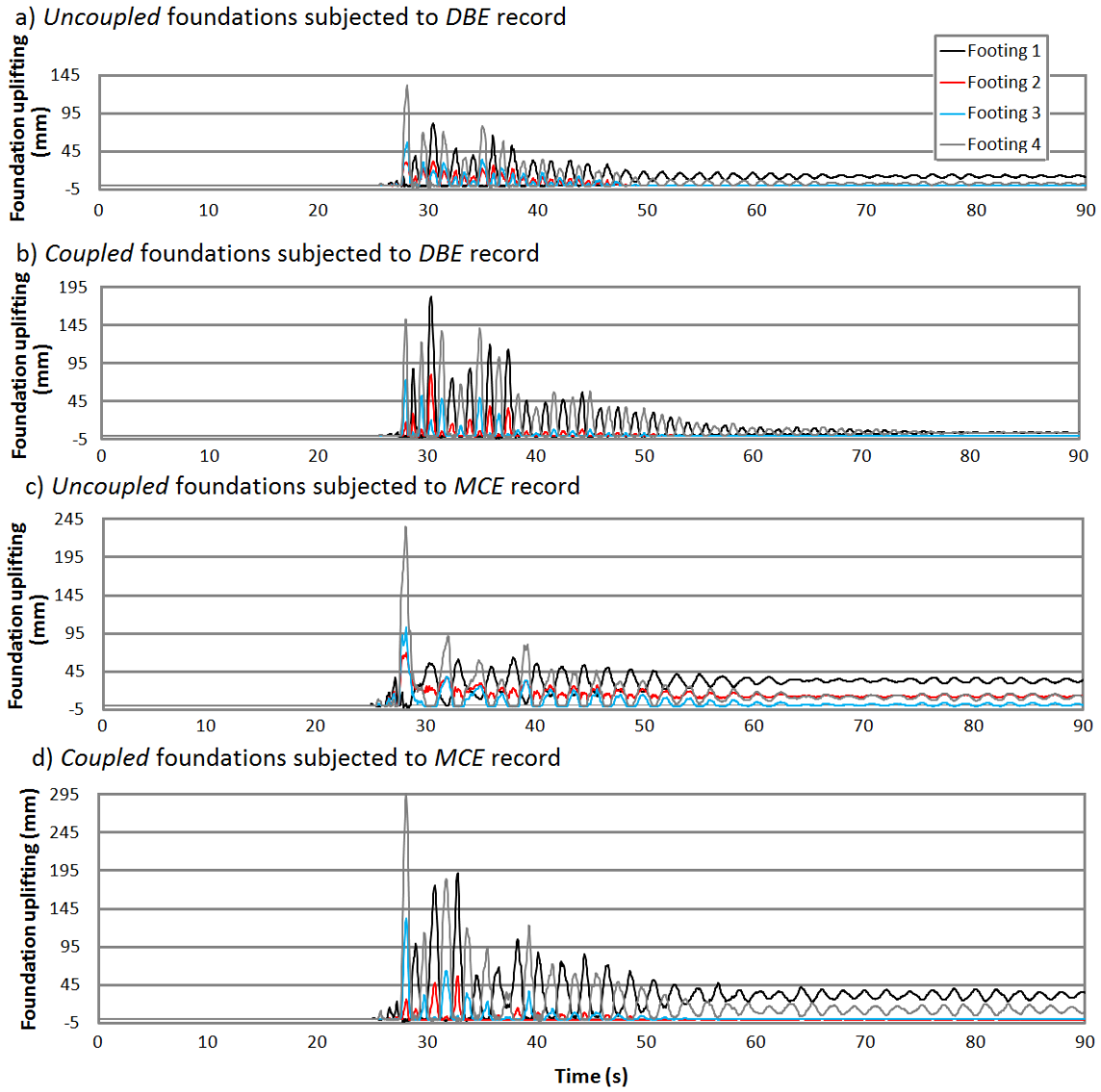


**Fig. 6:** Effect of tie beams on "uplifting" response of the footings at two different excitation levels

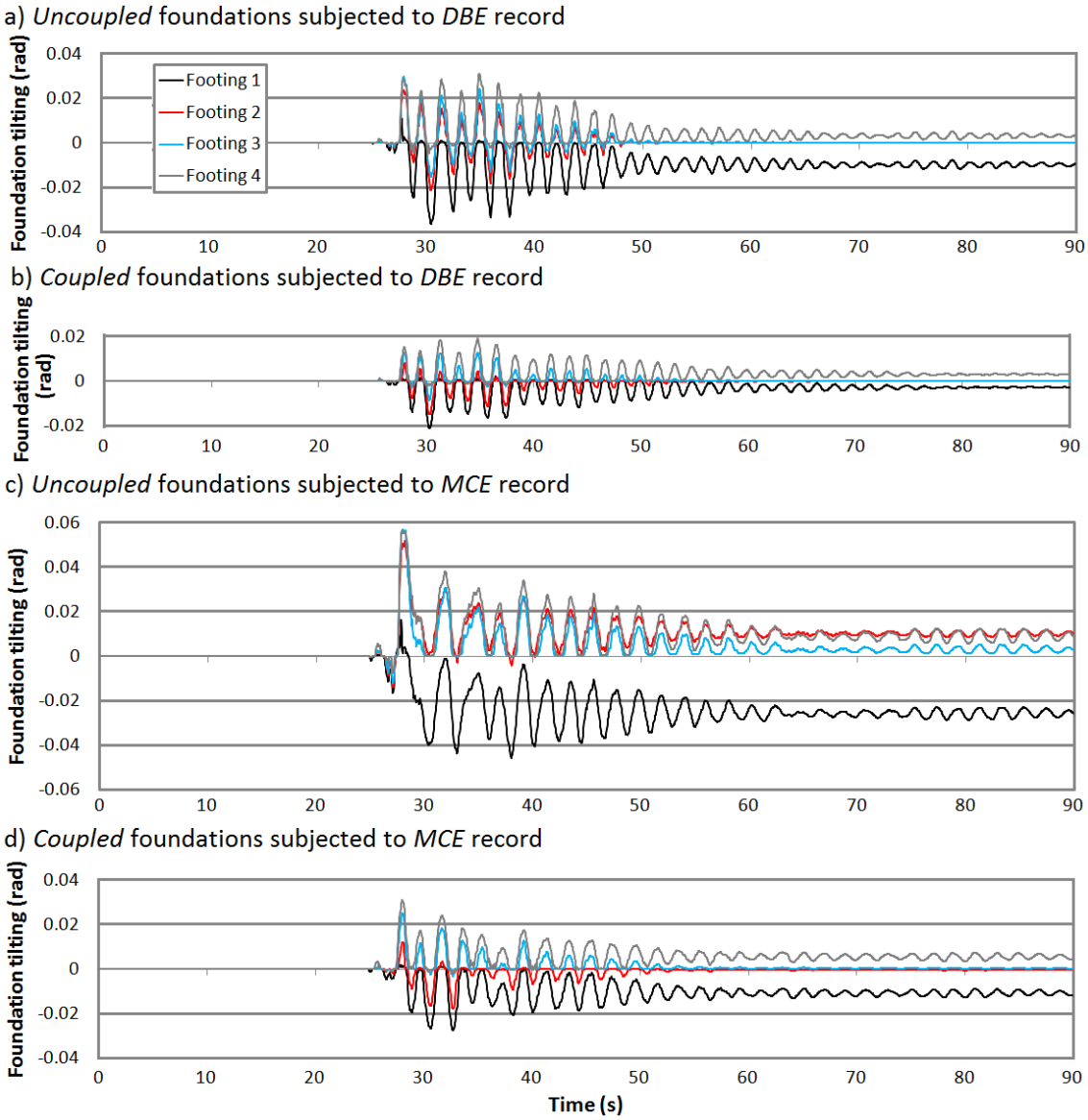


**Fig. 7:** Effect of tie beams on "rocking" response of the footings at two different excitation levels

## 8. Fragility Assessment

Assuming that the 27 real ground motions provide enough information to reliably estimate the parameters defining the fragility curve, the IDA analysis data are generated in the four cases, as introduced in section 6, comparatively. As a matter of fact, the rocking motions of the footings are not identical at a given arbitrary moment. This fact biases the damage estimation based exclusively on interstory drifts, especially at strong excitation levels, prior to the collapse of the structure. To solve this problem, a different damage measure is applied in this study which is based on moment-rotation hysteresis loops in plastic hinges.

### *8.1. Damage measure*

The Different types of damage models have been introduced by researchers in the last few decades. Considering realistic prediction of actual damage states as well as wide applicability of RC, steel [26,27] and timber [28] structures, in addition to compatibility with different hysteresis characteristics, the Park-Ang model is one of the most preferable choices as a structural damage index. The structural damage based on Park-Ang model, is a function of (i) the response i.e. maximum deformation of structure during an earthquake and hysteretic energy absorbed by building structure during NTHA that are both dependent on the loading history, and (ii) the parameters that specify the structural capacity. Values of the Park-Ang damage index greater than unity signifies collapse or total damage of the structure [29].

As a next step in the process of damage analysis, the calculated Park-Ang damage indices, denoted by $DI_{PA}$, should be related to some predefined damage states leading to an estimation of economic losses imposed on the structures. For this purpose, the following damage states are defined: (i) $DI_{PA} \leq 0.2$ representing Slight damage, (ii) $0.2 \leq$

$DI_{PA} \leq 0.4$ representing Moderate (repairable) damage, (iii) $0.4 \leq DI_{PA} \leq 1.0$ representing Extensive damage (beyond repair), and (iv) $1.0 \leq DI_{PA}$ representing loss of the structural component. The Park-Ang damage index $DI_{PA}$ can be obtained for an individual structural member (local damage index), for each story of the building (story damage index), and for the whole of the structure (global damage index). The story damage index, story $DI_{PA}$, and global damage index, *Global* $DI_{PA}$, can be calculated as the weighted average of the local damage indices, while the maximum total energy absorbed by each element would be weighting factor. In this study, the global damage indices are calculated for overall structural damage assessment purposes.

### *8.2. SSI effects on local as well as global damage indices*

Consider the 5-story steel MRF structure as described in section 3. As an illustrative example, the damage distribution within the frame is shown in Fig. 8 when the frame is typically subjected to fault-normal component (ps10_199) of 2002 Denali, Alaska, TAPS Pump Sta. #10 ground motion. The incident record is scaled to MCE (exceeding design limits). The SSI boundary conditions are denoted by cases 1 through 4 in Fig. 8, as introduced in section 6. A color spectrum is introduced to represent the local damage index of each member in Fig. 8. The global damage indices of each structure are also presented in Fig. 8. The moment-rotation history of a typical member is depicted in Fig. 9. These *M*-$\theta$ loops belong to left-end plastic hinge of the interior beam on the first floor as a representative structural member. As shown, the internal area of the loops is limited in nonlinear SSI condition. It is obvious that the nonlinear SSI has significantly reduced the damage state of the structure. On the other hand, damage state of the superstructure is enhanced when the footings are coupled (i.e. tie beams are used), so that the *Global* $DI_{PA}$ is reduced from 0.877 in case 3 to 0.560 in case 4, according to Fig. 8.

Comparing the damage indices shows that the beams which are responsible for structural energy dissipation of the MRF structure are significantly protected when nonlinear SSI is included, so that benefiting from rocking isolation effects, the irreparable damages in critical members of the fixed-base frame are lowered close to minor damage limit. In contrary, linear SSI (case 2 in Fig. 8), which means flexible-base foundation without uplifting and soil yielding, has a negligible contribution to the problem and does not attract attention as a key issue.

### *8.3. Extracting fragility curves from IDA results*

A fragility function specifies the probability of collapse, or some other limit state of interest of a structure as a function of some ground motion intensity measure, *IM*. The parameter *IM* is often quantified by spectral acceleration with a specified period and damping, though any measure of ground motion intensity can be used with the procedures below. Collapse fragility functions obtained from structural analysis results are increasingly popular in structural assessment procedures [21,30].

For a given ground motion and dynamic structural analysis result, the occurrence or nonoccurrence of collapse can be defined in a number of ways [31]. In this paper it is assumed that comparing *Global* $DI_{PA}$ to threshold 1.0 determines whether or not the ground motion caused collapse. The results below are not limited to collapse level only, and in fact any performance level of interest is assessed using its corresponding damage state according to thresholds given in Section 8.1. There are a number of procedures for performing nonlinear dynamic structural analyses to collect the data for estimating a fragility function. One common approach is incremental dynamic analysis (IDA), where a suite of ground motions are repeatedly scaled in order to find the *IM* level at which each ground motion causes collapse [21,32-33]. For fragility function fitting, an optimal strategy, as described below, must be followed in order to obtain an accurate fragility estimate with a minimal number of structural analyses.

In the case of analytical fragility functions, a lognormal cumulative distribution function is often used to define a fragility function:

$$P(C \mid IM = x) = \phi\left(\frac{\ln\left(x/\theta\right)}{\beta}\right) \quad (1)$$

where $P(C \mid IM = x)$ is the probability that a ground motion with $IM = x$ will cause the structure to collapse, $\Phi(\,)$ is the standard normal cumulative distribution function (CDF), $\theta$ is the median of the fragility function (the *IM* level with 50% probability of collapse) and $\beta$ is the standard deviation of ln*IM* (sometimes referred to as the dispersion of *IM*). Equation 1 implies that the *IM* values of ground motions causing collapse of a given structure are log-normally distributed. Calibrating equation 1 for a given structure requires estimating $\theta$ and $\beta$ from structural analysis results. We denote estimates of those parameters as $\hat{\theta}$ and $\hat{\beta}$. Parameter estimation is the field of statistics associated with estimating values of model parameters based on observed data that has a random component. In this case, our parameters of interest are $\theta$ and $\beta$, and we have randomness because record-to-record variability causes ground motions with the same *IM* level to produce different demands on a given structure.

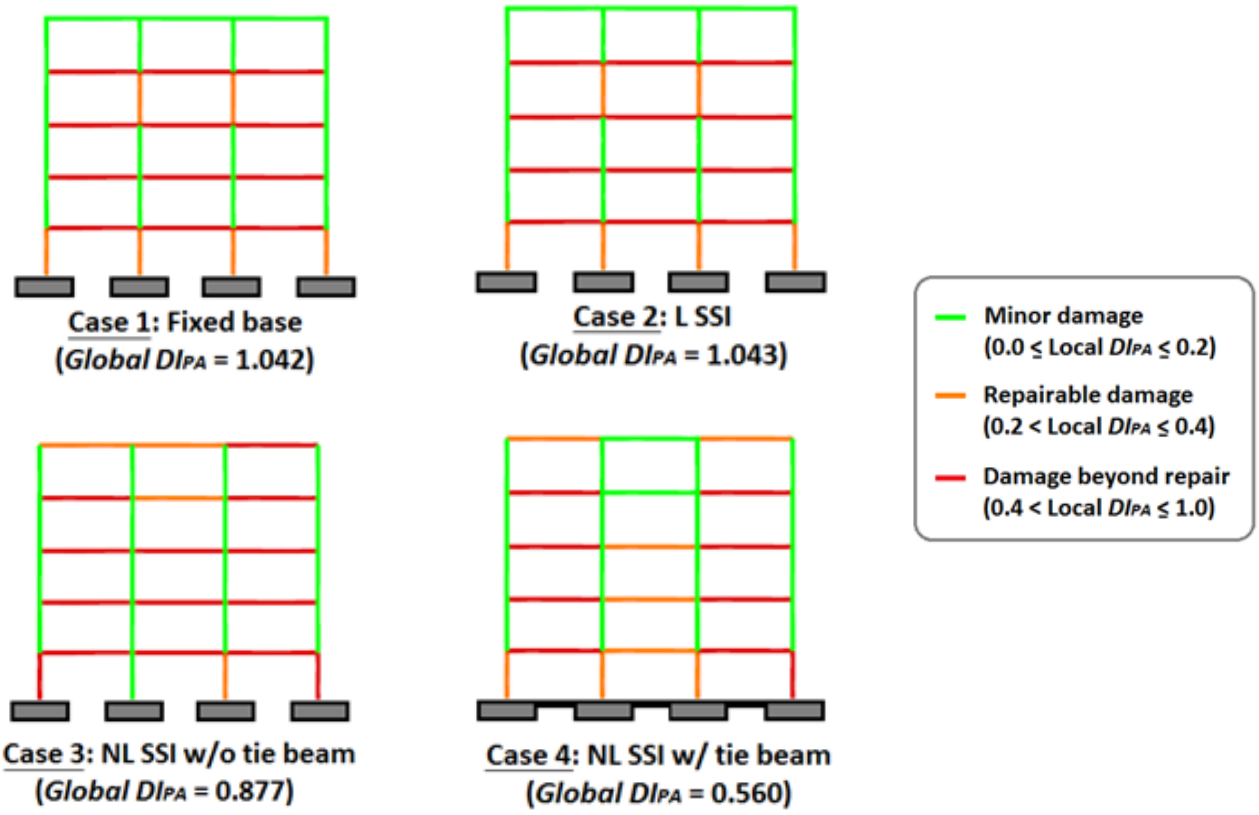


**Fig. 8:** Typical distribution of local damage indices over the structural members

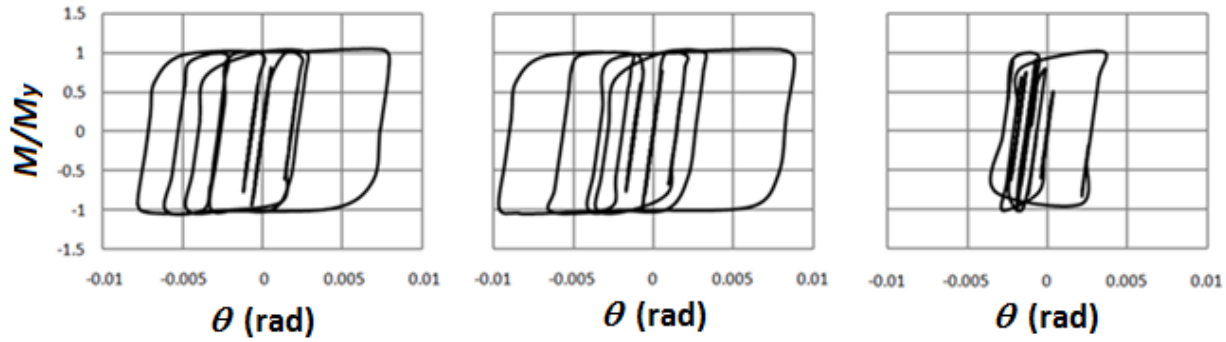


**Fig. 9:** Moment-rotation hysteresis loops at left-end plastic hinge of a typical beam member: a) Fixed-base (case 1), b) Linear SSI (case 2), and c) Nonlinear SSI without tie beams (case 3).

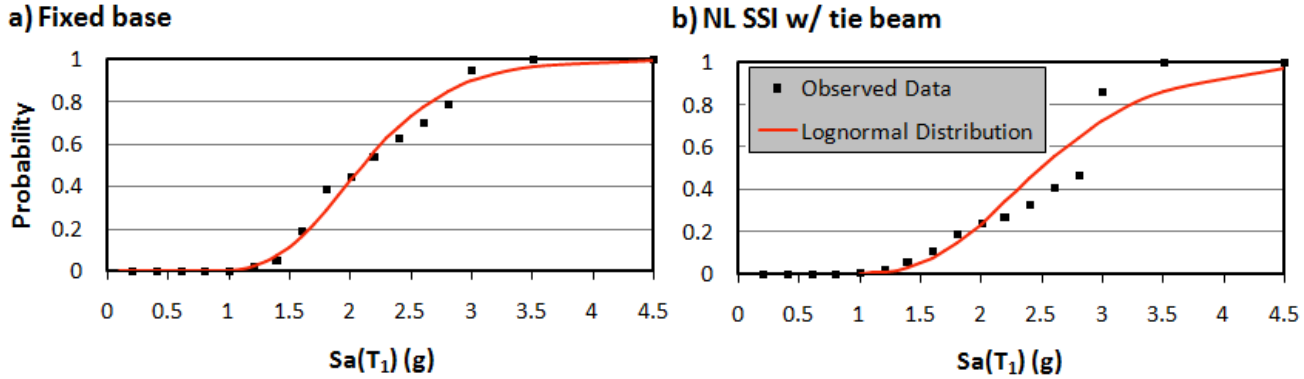


**Fig. 10:** Extracting fragility curves with the best fit to the statistical data points (two different SSI conditions are compared for illustrative purposes)

There are a number of ways to estimate parameter values for a fragility function that are consistent with observed data, depending upon the procedure used to obtain structural analysis data.

IDA is the procedure used in this study to obtain the analysis data. Incremental dynamic analysis (IDA) involves scaling each ground motion in a suite until it causes collapse of the structure [32]. This process produces a set of *IM* values associated with the onset of collapse for each ground motion. The probability of collapse at a given *IM* level, *x*, can then be estimated as the fraction of records for which collapse occurs at a level lower than *x*. Fragility function parameters can be estimated from this data by taking logarithms of each ground motion's *IM* value associated with onset of collapse, and computing their mean and standard deviation, as follows:

$$\ln \theta = \frac{1}{n}\sum_{i=1}^{n} \ln IM_i \quad (2)$$

$$\beta = \sqrt{\frac{1}{n-1}\sum_{i=1}^{n}\left(\ln\left(IM_i / \theta\right)\right)^2} \quad (3)$$

where n is the number of ground motions considered, and $IM_i$ is the *IM* value associated with onset of collapse for the ith ground motion. This is a method of moments estimator, as $\ln\theta$ and $\beta$ are the mean and standard deviation, respectively, of the normal distribution representing the ln*IM* values. Note that the mean of ln*IM* is equal to the median of *IM* in the case that *IM* is lognormally distributed, which is why using the sample mean in this manner produces an estimate of $\theta$. The mean and standard deviation, or moments, of the distribution are estimated using the sample moments from a set of data. Fragility function fitted using this approach is shown in Fig. 10 for fixed-base structure (case 1) as well as nonlinear SSI condition and coupled foundation (case 4). These damage states are derived for the highest damage state corresponding to *Global* $DI_{PA} \geq 1.0$ which represents building collapse.

### *8.4. Fragility curves at different damage states*

The fragility curves for the first to fourth damage states (i.e. Slight, Moderate, Extensive, and Complete damage as introduced in section 8.1) are computed while the different SSI boundary conditions are compared. The derived fragility curves are presented in Fig. 11. Evidently, the fragility curves agree with the tendencies of the dynamical responses as described in section 6, i.e. a general reduction is observed when nonlinear SSI effects are included. This reduction of the structural demand is related to the combined effect of radiation damping, modification of vibrating modes and hysteretic damping of soil due to its nonlinear behavior i.e. foundation uplifting and soil yielding. Considering the slight damage state, a reduction of near to 50% of the probability to reach this damage state is obtained for motion with $S_a(T_1) < 0.5$g. This difference decreases gradually as the severity of the motion increases. Regarding the moderate state level, the fragility curves start approximately at $S_a(T_1) = 0.6$g, nevertheless, the probability to reach the moderate damage state is reduced up to 40% when nonlinear SSI effects are included in the analysis. This difference decreases gradually for motions with $S_a(T_1) = 2.0$g. In this case, SSI effects are still favorable to reduce seismic demand under moderate damage state threshold at strong motions. At extensive damage state level, the fragility curves start approximately at $S_a(T_1) = 0.8$g. The probability to reach the extensive damage state is reduced up to 45% when nonlinear SSI effects are included. This difference decreases gradually for motions with $S_a(T_1) = 2.7$g. At the highest damage state, namely complete damage, the fragility curves start approximately at $S_a(T_1) = 1.2$g. The probability to reach the complete damage state is reduced up to 10% when nonlinear SSI effects are included and the foundation is uncoupled. This reduction is more intensified in nonlinear SSI condition while the foundation is integrated with tie beams. In such condition, thanks to the application of tie beams, the greatest beneficial effects (up to 20%) on enhancing the seismic demands are captured under complete damage state threshold.

As stated before in section 5, a suite of 27 records are used as input ground motion in this study. Among these ground motions, 12 records are near field pulse like, 8 of them are near field without pulse and the remaining are classified as far field records. To assess the effect of ground motion type on seismic structural damage, a set of fragility curves are derived for each type of ground motion separately, as illustrated in Figs. 12 and 13. According to results of Figs. 12 and 13, it is concluded that near field pulse like records are more destructive than far field or near field no-pulse records in terms of fragility curves. For instance (see Fig. 12), the probability of exceeding limits of "Extensive" damage state is equal to 59.2% in case of nonlinear soil-structure with tie beams subjected to near field pulse-like records with intensity of Sa(T1)=2g. The corresponding probability values are equal to 24.8% and 15.3% in case of near field no-pulse and far field records, respectively. Similarly, according to Fig. 13, the probability of exceeding limits of "Collapse" damage state is equal to 32.0% in case of nonlinear soil-structure with tie beams subjected to near field pulse-like records with intensity of Sa(T1)=2g. The corresponding probability values are equal to 21.0% and 15.1% in case of near field no-pulse and far field records, respectively.

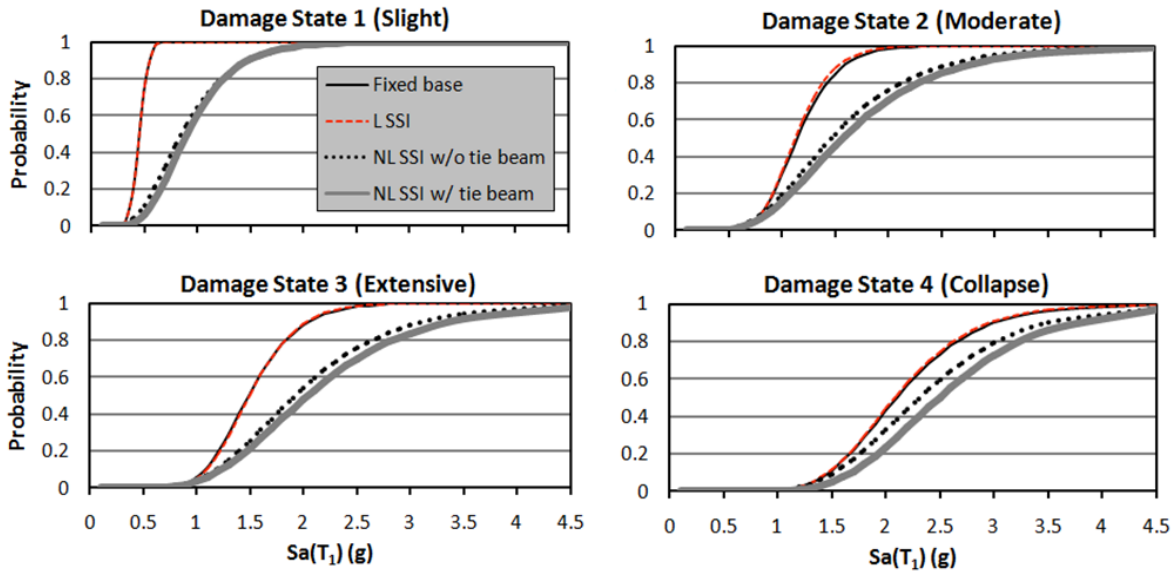


**Fig. 11:** Computed fragility curves at different damage states as well as different SSI conditions

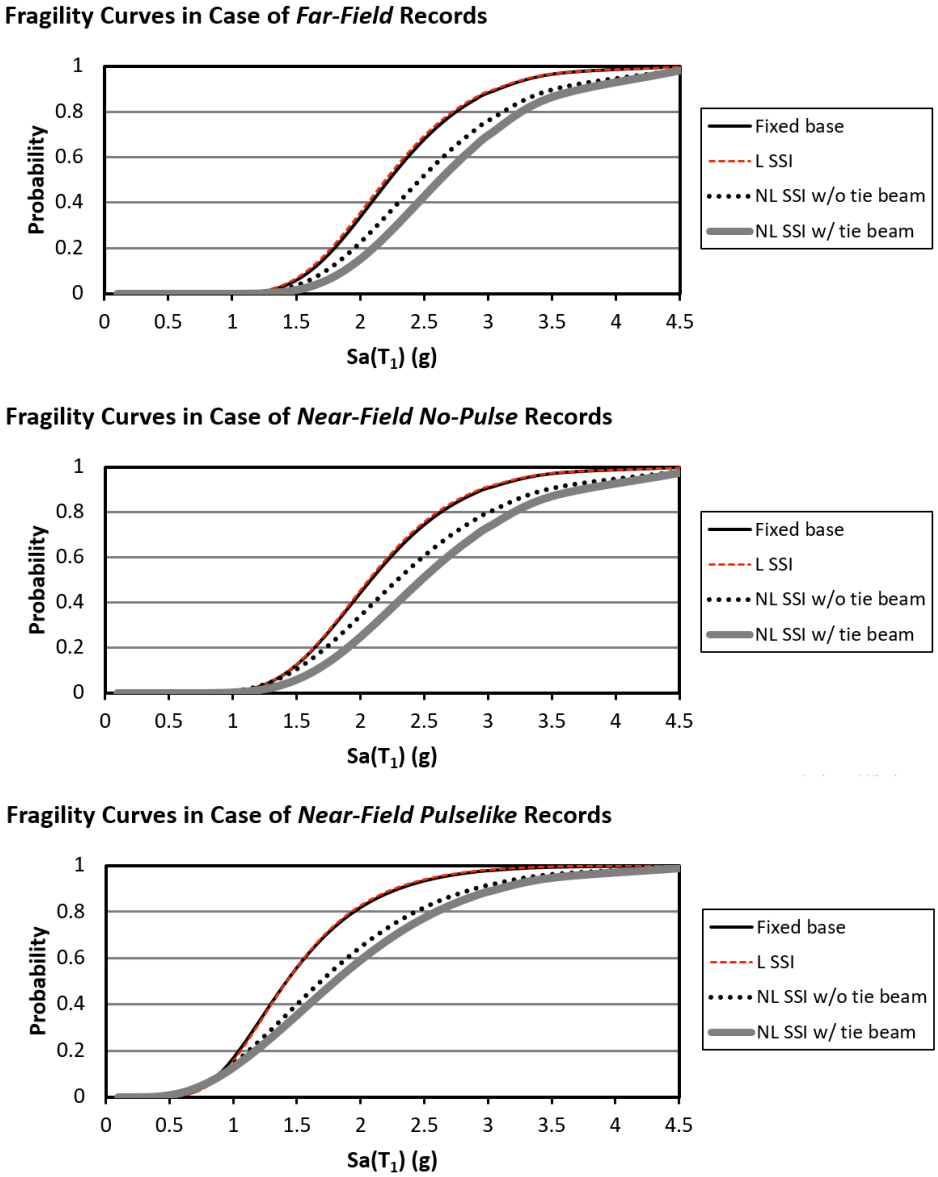


**Fig. 12:** Comparative fragility curves at "Extensive" damage state in case of different seismic input ground motions

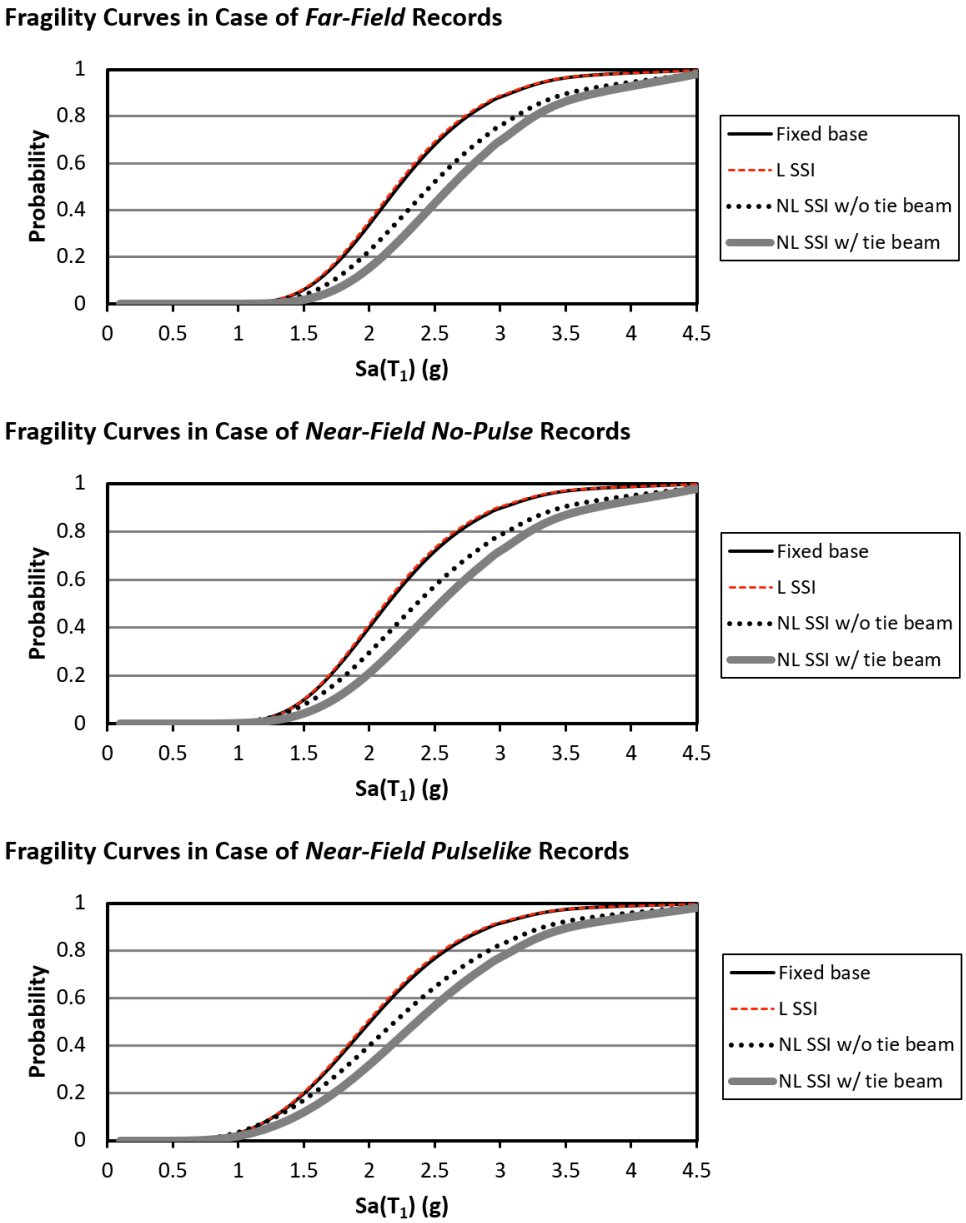


**Fig. 13:** Comparative fragility curves at "Collapse" damage state in case of different seismic input ground motions

The comparison between the developed fragility model in this study for the 5-story steel MRF with the corresponding one in HAZUS [2] is carried out in Fig. 14. For this purpose, the maximum interstory drifts derived from NTHAs are compared with HAZUS criteria to determine number of meeting or exceeding the limit states. Evidently, the HAZUS method yields a reduced probability of exceedance compared to the proposed fragility curves. The difference between the curves increases in case of more severe damage states. So, the most significant difference is almost equal to 32%, which occurs in the case of nonlinear soil-structure with tie beams at "Collapse" damage state.

Interestingly, nonlinear SSI effects have narrowed the gap between the proposed and HAZUS fragility curves. In other words, incorporation of nonlinear SSI including soil yielding and foundation uplifting has led to fragility curves, which are closer to the well-known HAZUS fragility functions. The compatibility between proposed versus HAZUS fragility curves is greatly manifested at "Slight" as well as "Moderate" damage states, as displayed in Fig. 14. In a statistical context, the agreement between the fragility curves derived for the example building studied in this paper are quite satisfactory. As expected, the derived fragility curves provide a reliable quantification of the effects of the nonlinear SSI on the seismic vulnerability assessment of the considered building. Further investigations of this kind will be needed in order to obtain more general conclusions for diverse building typologies, foundation systems and soil types.

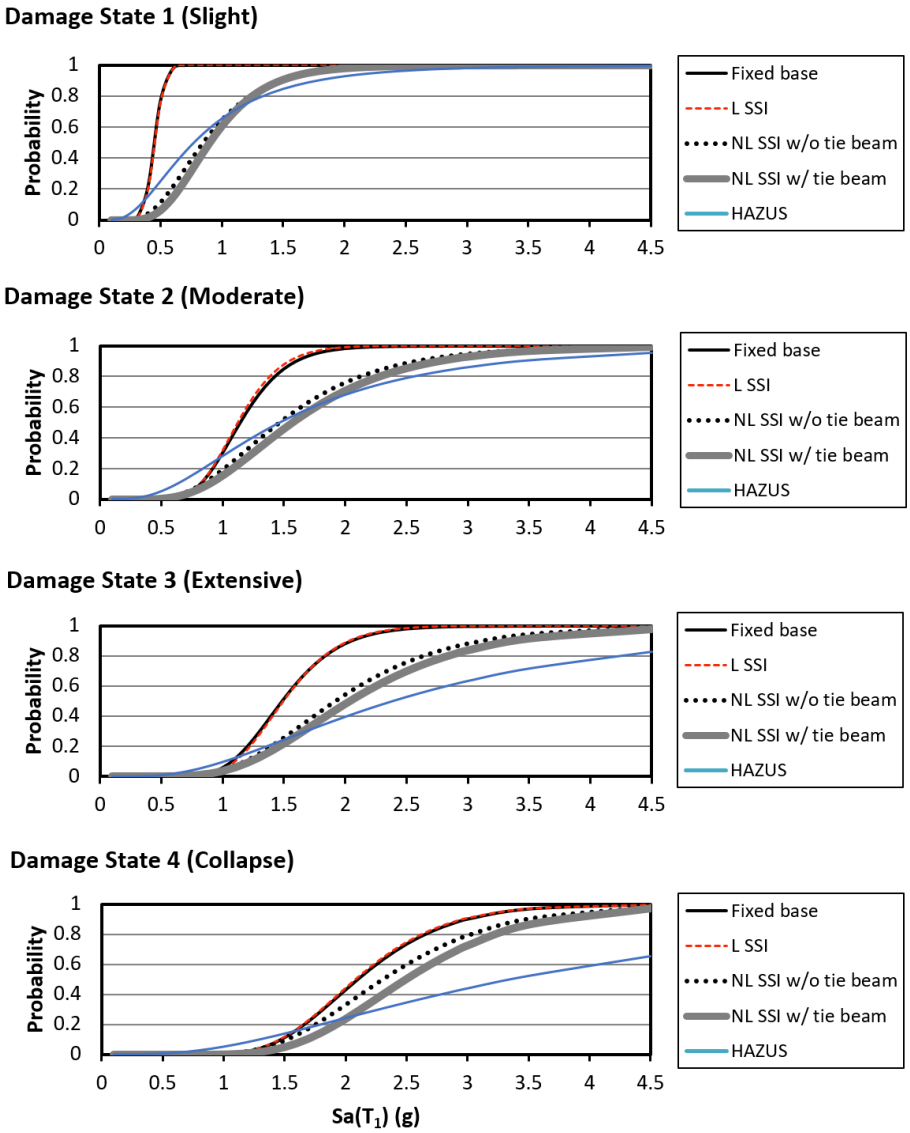


**Fig. 14:** Comparison of the proposed fragility curves for the 5-story steel MRF with the corresponding one in HAZUS

## 9. Conclusions

A study on the influence of nonlinear SSI on the assessment of the seismic vulnerability of steel buildings is presented in this paper. Two major aspects have been exposed. The first refers to the effects of foundation uplifting and soil yielding by which the plastic hinge formation would be induced within the underlying soil and consequently the superstructure remains protected. The second examines the role of foundation system in NTHA-based damage estimation. To this end, application of tie beams is evaluated and two sets of fragility curves are compared at different damage states. The modeling of nonlinear SSI is performed using the modified Beam-on-Nonlinear Winkler Foundation (BNWF).

According to the findings of this study, there is a reduction in seismic demands in general when nonlinear SSI is included. This reduction can be associated fundamentally with two phenomena: radiation damping and hysteretic damping due to foundation uplifting and soil yielding. Evidently, the results of some existing time-history analyses performed in this study manifest unexpected increases in structural demands. Accordingly, it might be too soon to over-generalize the observations. A set of modified fragility curves dealing with SSI effects are derived, by which more realistic seismic loss estimations would be possible. These modification factors need to be generalized with respect to diverse structure, foundation, and soil typologies.

## References

**[1]** Federal Emergency Management Agency. Earthquake damage evaluation data for California (ATC 13). Applied Technology Council; 1985.

**[2]** Federal Emergency Management Agency. Multi-hazard loss

estimation methodology, earthquake model, HAZUS-MH MR4 technical manual. 2003.

**[3]** Cavalieri F, Correia AA, Crowley H, Pinho R. Seismic fragility analysis of URM buildings founded on piles: influence of dynamic soil–structure interaction models. Bull Earthq Eng 2020;18:4127–56.

**[4]** Salami MR, Kashani MM, Goda K. Influence of advanced structural modeling technique, mainshock-aftershock sequences, and ground-motion types on seismic fragility of low-rise RC structures. Soil Dyn Earthq Eng 2019;117:263–79.

**[5]** Segura R, Padgett JE, Paultre P. Metamodel-based seismic fragility analysis of concrete gravity dams. J Struct Eng 2020;146:4020121.

**[6]** Ellingwood BR, Celik OC, Kinali K. Fragility assessment of building structural systems in Mid-America. Earthq Eng Struct Dyn 2007;36:1935–52.

**[7]** Cavalieri F, Correia AA, Crowley H, Pinho R. Dynamic soil-structure interaction models for fragility characterisation of buildings with shallow foundations. Soil Dyn Earthq Eng 2020;132:106004.

**[8]** Sáez E, Lopez-Caballero F, Modaressi-Farahmand-Razavi A. Effect of the inelastic dynamic soil–structure interaction on the seismic vulnerability assessment. Struct Saf 2011;33:51–63.

**[9]** Japan International Cooperation Agency. The study on seismic microzoning of the Greater Tehran Area in the Islamic Republic of Iran. Pacific Consult Int Report, OYO Coop Japan 2000:291–390.

**[10]** Mansouri B, Ghafory-Ashtiany M, Amini-Hosseini K, Nourjou R, Mousavi M. Building seismic loss model for Tehran. Earthq Spectra 2010;26:153–68.

**[11]** American Society of Civil Engineers. Minimum design loads for buildings and other structures (ASCE 7) 2010.

**[12]** American Institute of Steel Construction. Specification for structural steel buildings (ANSI/AISC 360). 2010.

**[13]** McKenna F, Fenves GL, Scott MH. Open system for earthquake engineering simulation. Univ California, Berkeley, CA 2000. http://opensees.berkeley.edu.

**[14]** Ibarra LF, Krawinkler H. Global collapse of frame structures under seismic excitations. Pacific Earthquake Engineering Research Center Berkeley, CA; 2005.

**[15]** Lignos DG, Krawinkler H. Deterioration Modeling of Steel Components in Support of Collapse Prediction of Steel Moment Frames under Earthquake Loading. J Struct Eng 2011;137:1291–302.

**[16]** Gajan S, Raychowdhury P, Hutchinson TC, Kutter BL, Stewart JP. Application and validation of practical tools for nonlinear soil-foundation interaction analysis. Earthq Spectra 2010;26:111–29.

**[17]** Harden CW, Hutchinson TC. Beam-on-nonlinear-Winkler-foundation modeling of shallow, rocking-dominated footings. Earthq Spectra 2009;25:277–300.

**[18]** Harden CW. Numerical modeling of the nonlinear cyclic response of shallow foundations. Pacific Earthquake Engineering Research Center; 2005.

**[19]** Raychowdhury P, Hutchinson T. Nonlinear material models for Winkler-based shallow foundation response evaluation. GeoCongress 2008 Charact. Monit. Model. GeoSystems, 2008, p. 686–93.

**[20]** Gajan S, Hutchinson TC, Kutter BL, Raychowdhury P, Ugalde JA, Stewart JP. Numerical models for analysis and performance-based design of shallow foundations subjected to seismic loading. Pacific Earthquake Engineering Research Center Berkeley; 2008.

**[21]** Federal Emergency Management Agency. Quantification of building seismic performance factors (FEMA P695). Applied Technology Council; 2009.

**[22]** Baker JW. Quantitative classification of near-fault ground motions using wavelet analysis. Bull Seismol Soc Am 2007;97:1486–501.

**[23]** Road, Housing, and Urban Development Research Center. Iranian code of practice for seismic resistant design of buildings. 2014.

**[24]** Al-Mashaykhi M, Rajeev P, Wijesundara KK, Hashemi MJ. Displacement profile for displacement based seismic design of concentric braced frames. J Constr Steel Res 2019;155:233–48.

**[25]** Shoeibi S, Kafi MA, Gholhaki M. New performance-based seismic design method for structures with structural fuse system. Eng Struct 2017;132:745–60.

**[26]** Ghosh S, Datta D, Katakdhond AA. Estimation of the Park–Ang damage index for planar multi-storey frames using equivalent single-degree systems. Eng Struct 2011;33:2509–24.

**[27]** Park Y-J, Ang AHS, Wen YK. Damage-limiting aseismic design of buildings. Earthq Spectra 1987;3:1–26.

**[28]** Van de Lindt JW. Damage-based seismic reliability concept for woodframe structures. J Struct Eng 2005;131:668–75.

**[29]** Park Y-J, Ang AH-S. Mechanistic seismic damage model for reinforced concrete. J Struct Eng 1985;111:722–39.

**[30]** Applied Technology Council. Seismic performance assessment of buildings. Federal Emergency Management Agency; 2012.

**[31]** Zareian F, Krawinkler H. Assessment of probability of collapse and design for collapse safety. Earthq Eng Struct Dyn 2007;36:1901–14.

**[32]** Vamvatsikos D, Cornell CA. Incremental dynamic analysis. Earthq Eng Struct Dyn 2002;31:491–514.

**[33]** Harati M, Mashayekhi M, Barmchi MA, Estekanchi H. Influence of Ground Motion Duration on the Structural Response at Multiple Seismic Intensity Levels. Numerical Methods in Civil Engineering Journal 2019; 3(4):10-23.